Few-mode optical fiber surface plasmon resonance sensor with controllable range of measured refractive index

Wael Abu Shehab[1], Ahmad Salah[1], Wael Al-Sawalmeh[2], Haitham Alashaary[3]
[1]Department of Electrical Engineering, Al-Hussein Bin Talal University, Maan, Jordan
[2]Department of Communications Engineering, Al-Hussein Bin Talal University, Maan, Jordan
[3]Department of Computer Engineering, Al-Hussein Bin Talal University, Maan, Jordan

Article Info

Article history:

Received Jan 11, 2022
Revised Jul 14, 2022
Accepted Aug 26, 2022

Keywords:

Few-mode
Graphene
Optical fiber sensor
Refractive index
Sensitivity

ABSTRACT

A few-mode optical fiber surface plasmon resonance sensor with graphene layer is investigated, firstly, with the aim of studying the behavior of the guided modes and, secondly, with the aim of determining the range of the measured refractive index for some selected few-mode fibers. The results show that as the number of modes propagated in the fiber increases, the maximum sensitivity of a particular mode decreases while the range of the measured refractive index of that mode increases. Also, it is shown that the range can be easily tuned with sensitivity consideration by only adjusting the operating wavelength without any modification of the sensor, which is desirable from practical point of view. In addition, it is shown that the core diameter of the fiber should be chosen according to sensitivity and range needing, where a compromise between them must be found. The study presented in this paper can significantly help in developing new sensing techniques, such as multi-parameter sensing, by monitoring the various responses of the modes. Also, it can be used to customize the sensor for specific sensing applications in various fields, especially to measure refractive indices in subranges of 1.38 to 1.46.

Corresponding Author:

Wael Abu Shehab
Department of Electrical Engineering, Al-Hussein Bin Talal University
Maan 71111, Jordan
Email: waelabushehab@ahu.edu.jo

1. INTRODUCTION

Optical fiber sensors have been intensively investigated and reviewed in many research due to their high performance and unique capabilities [1], [2]. One of their uses is refractive index detection [3]–[6], which is significantly important in various fields. In recent years, optical fiber surface plasmon resonance (SPR) sensors have achieved a high impact due to their high performance. They have been used in various sensing applications, such as biosensing [7], disease diagnosis [8], corrosion monitoring [9], water quality detection [10], and liquid detection [11], [12]. Researchers have developed distinct structures of these sensors in order to enhance their sensing performance. A dual-truncated-cone structure of a fiber is used for excitation and reception of SPR signals in [13], where a Bessel-like beam is used as input source. Kadhim *et al.* [5] proposed a single-mode fiber SPR sensor using a multiple D-shaped Ag nanowire. A photonic crystal fiber SPR sensor is reported in [14], where a D-shaped sensor with V-groove analyte channel has been created. Hu *et al.* [3] proposed a fiber optic SPR refractive index sensor based on multimode-no-core-multimode fiber structure. A core-shift welding technology has been investigated in [15], where a light is directly injected into the sensing fiber cladding to obtain the evanescent field at the interface between the cladding and the air. Several types of optical fiber grating-based SPR sensors have also been proposed such as in [16]–[18].

Recently, many two-dimensional materials have been discovered to enhance the optical fiber SPR sensors performance. Among these materials is graphene, which has attracted high attention due to its superior performance. Nurrohman and Chiu [19] discussed the properties of graphene in general, its use in sensors, and current status and future prospects of graphene-based SPR sensors. Different configurations of graphene based SPR sensors have been investigated and designed to enhance the sensor performance. Zhou *et al.* [12] have designed an end reflection optical fiber SPR sensor, where one end of the fiber has been coated by silver film and graphene. In [20], SPR sensor based on photonic crystal fiber coated with a graphene layer was designed and numerically analyzed. A D-shape plastic optical fiber SPR sensor based on graphene/gold film has been investigated in [21]. Another D-shaped single-mode fiber SPR sensor has been proposed in [22] using composite nanostructure of MoS2-graphene.

To the best of our knowledge, no studies have investigated the role of each guided mode and its contribution to the SPR sensor's performance. This is very important since monitoring the various responses of the modes may significantly develop new sensing techniques, such as enabling simultaneous measurements of multiple parameters [1]. In the previous work [23], the performance of the fundamental linear polarized (LP_{01}) mode in optical fiber SPR sensor has been studied for different operating wavelengths, where the study was related only to single-mode fiber. In this paper, the performance of guided modes in SPR sensor is examined for some selected few-mode fibers, which are an ideal compromise between single-mode and multimode fibers [24]. The study is applied on a D-shaped sensor structure with graphene layer due to its superior performance as mentioned earlier. However, it can also be applied, in a similar way, to other structures with different numbers and types of layers. The effect of changing the operating wavelength on the range of the measured refractive index and the sensitivity is investigated for some selected few-mode fibers. In addition, different thicknesses of graphene, metal, and residual cladding have been examined. The paper is carried out in four sections starting with the introduction. Section 2 describes sensor structure and modeling, followed by results and discussion in section 3. Finally, the conclusion is presented in section 4.

2. STRUCTURE DESIGN AND MODELING

The proposed D-shaped sensor is shown in Figure 1, where the cross-sectional view of the sensor and its detailed structure are illustrated in Figures 1(a) and 1(b), respectively. The proposed sensor is designed by side polishing a step-index fiber. The diameter of the core and the thickness of the residual cladding are d_1 and d_2, respectively. The length of the sensing region is l. The side-polished cladding is covered with a metal layer of d_3 thickness. Graphene layers are placed over the metal layer in order to examine the sensor's performance enhancement. The thickness of these layers is d_4. The single layer thickness of graphene is 0.34 nm [24]. Thus, d_4 can be expressed as $d_4 = L \times 0.34\,nm$, where L is the number of graphene layers. The core, cladding, metal, graphene, and analyte refractive indices are denoted as $n_1, n_2, n_3, n_4,$ and n_5, respectively. The core and cladding refractive indices are determined using the well-known equation [25], [26],

$$n^2(\lambda) = 1 + \frac{a_1\lambda^2}{\lambda^2 - b_1^2} + \frac{a_2\lambda^2}{\lambda^2 - b_2^2} + \frac{a_3\lambda^2}{\lambda^2 - b_3^2} \tag{1}$$

where λ is the wavelength of the incident light in micrometers, and $a_1, a_2, a_3, b_1, b_2,$ and b_3 are Sellmeier coefficients.

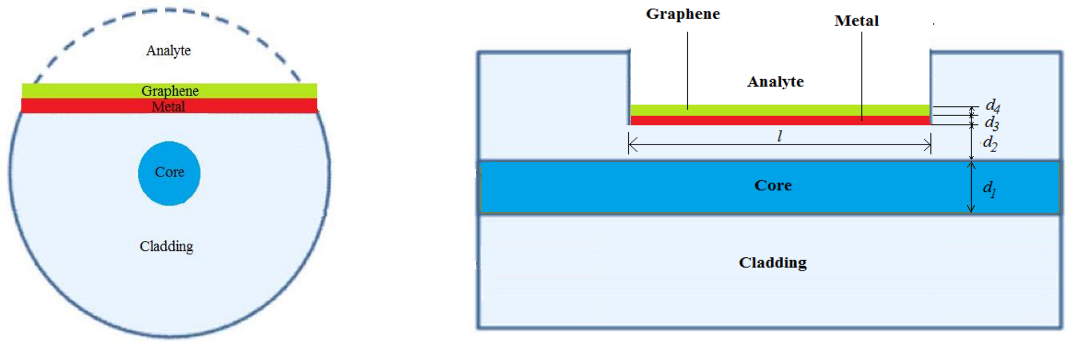

(a) (b)

Figure 1. The proposed D-shaped sensor: (a) cross-sectional view and (b) detailed structure

Due to chemical stability of gold, it is used to be the metal layer in the sensor structure. To determine the wavelength-dependent refractive index of the gold, different models can be found in research. In this paper, a Lorentz-Drude model with two additional Lorentzian terms [27] has been adopted, where the accuracy of this model is sufficient and suitable over the spectral range used in our work. According to this model, the refractive index of the metal n_3 is expressed by (2) [27],

$$n_3 = \sqrt{1 - \frac{1}{\lambda_p^2\ (1/\lambda^2 + i/\gamma_p\lambda)} - \sum_{j=1}^{2} \frac{A_j}{\lambda_j^2\ (1/\lambda^2 - 1/\lambda_j^2) + i\ \lambda_j^2/\gamma_j\lambda}} \tag{2}$$

where λ_p and γ_p are Drude term parameters, A_j, λ_j, and γ_j are parameters of first $(j = 1)$ and second $(j = 2)$ Lorentz oscillators. The refractive index of graphene is obtained from (3) [24],

$$n_4 = 3 + \frac{iC\lambda}{3} \tag{3}$$

where constant $C \approx 5.446\mu m^{-1}$ and the light wavelength $\lambda$is given in micrometers.

To examine the performance of the individual modes propagating in the fiber and their contribution to the sensitivity of the SPR sensor, intensity interrogation technique is used, where the wavelength is kept fixed and thus the number of the propagating modes in the fiber can be determined and controlled by the value of the normalized frequency V. The analysis in this research is provided for linear polarized LP modes. Each of these modes has distinct value of propagation constant β, denoted as β_{lm}, where subscripts l and m characterize azimuthal and radial mode distribution, respectively. The mode of a specific value of β_{lm} is denoted as LP_{lm}. The propagation constants can be determined by solving the characteristic equation [28],

$$u\,\frac{J_{l\pm1}(u)}{J_l(u)} = \pm w\,\frac{k_{l\pm1}(w)}{k_l(w)} \tag{4}$$

where J_l is the Bessel function of the first kind and order l, k_l is the modified Bessel function of the second kind and order l, and u and w are the normalized transverse propagation constants for which it holds that $u^2 + w^2 = V^2$.

To examine the role of each of the propagating modes on the sensor performance, the reflectivity for each propagating mode should be determined. The reflectivity R' for a single reflection of the five-layer structure shown in Figure 1 can be written as (5) [29],

$$R' = \left|\frac{r_{12}A + B}{A + r_{12}B}\right|^2 \tag{5}$$

where

$$A = 1 + r_{23}r_{34}e^{j2k_3d_3} + r_{34}r_{45}e^{j2k_4d_4} + r_{23}r_{45}e^{j2(k_3d_3 + k_4d_4)} \tag{6}$$

$$B = r_{23}e^{j2k_2d_2} + r_{23}r_{34}r_{45}e^{j2(k_2d_2 + k_4d_4)} + r_{34}e^{j2(k_2d_2 + k_3d_3)} + r_{45}e^{j2(k_2d_2 + k_3d_3 + k_4d_4)} \tag{7}$$

$$r_{ij} = \frac{k_i/n_i^2 - k_j/n_j^2}{k_i/n_i^2 - k_j/n_j^2} \tag{8}$$

for $i = 1, 2, 3, 4$ and $j = i + 1$,

$$k_{i(or\ j)} = \frac{2\pi}{\lambda}\sqrt{n_{i(or\ j)}^2 - n_1^2 sin^2\theta} \tag{9}$$

and θ is the angle of the incident light with respect to the normal to the core-cladding interface and can be determined as provided in [23].

The total reflectivity R for the sensor of sensing length l and with number of reflections m is determined using (10) [29],

$$R = R'^m \tag{10}$$

where $m = l/(2d_1 tan\theta)$. Since intensity interrogation technique is used in this study, the sensor sensitivity S is determined by (11) [29].

$$S = \left|\frac{\partial R}{\partial n_5}\right| \tag{11}$$

3. RESULTS AND DISCUSSION

By reference to Figure 1, the core diameter d_1, residual cladding thickness d_2, metal thickness d_3, graphene layer thickness d_4, and sensing length l are taken to be 10 μm, 10 nm, 30 nm, 34 nm, and 4mm respectively. The Sellmeier coefficients appearing in (1) have values for undoped silica core and Fluorine-doped silica cladding according to [25]. The Lorentz-Drude parameters in (2) have values according to [27].

Figure 2 shows the performance of LP_{01} mode shown in Figure 2(a), LP_{11} mode shown in Figure 2(b), LP_{21} mode shown in Figure 2(c), and LP_{31} mode shown in Figure 2(d) for different wavelengths. Each of these wavelengths supports propagation of a few modes in the fiber. It is seen that the maximum sensitivity of a particular mode decreases as the wavelength decreases. In other words, as the number of modes propagated in the fiber increases, the maximum sensitivity of a particular mode decreases. It can be noticed that the sensitivity reaches small values for the guided modes in five-mode and six-mode fibers compared with the sensitivity values for the guided modes in fibers that support propagation of fewer number of modes. Also, comparing values of the maximum sensitivity for different propagating modes at a certain wavelength, it can be seen that as the order of the mode increases, the value of the maximum sensitivity increases. For example, at wavelength 850 nm (which supports propagation of LP_{01} and LP_{11} modes), the maximum sensitivity for LP_{01} mode is 645.3 RIU^{-1}, while it is 915.2 RIU^{-1} for LP_{11} mode. The modes performance in a fiber that supports propagation of two modes at 850 nm, and four modes at 620 nm, is shown in Figures 3 and 4, respectively. The mentioned results can also be illustrated by showing the dependence of sensitivity on wavelength for a certain analyte refractive index. Figure 5 illustrates this dependence for $n_5 = 1.430$ for two-mode and four-mode fibers as shown in Figures 5(a) and 5(b), respectively.

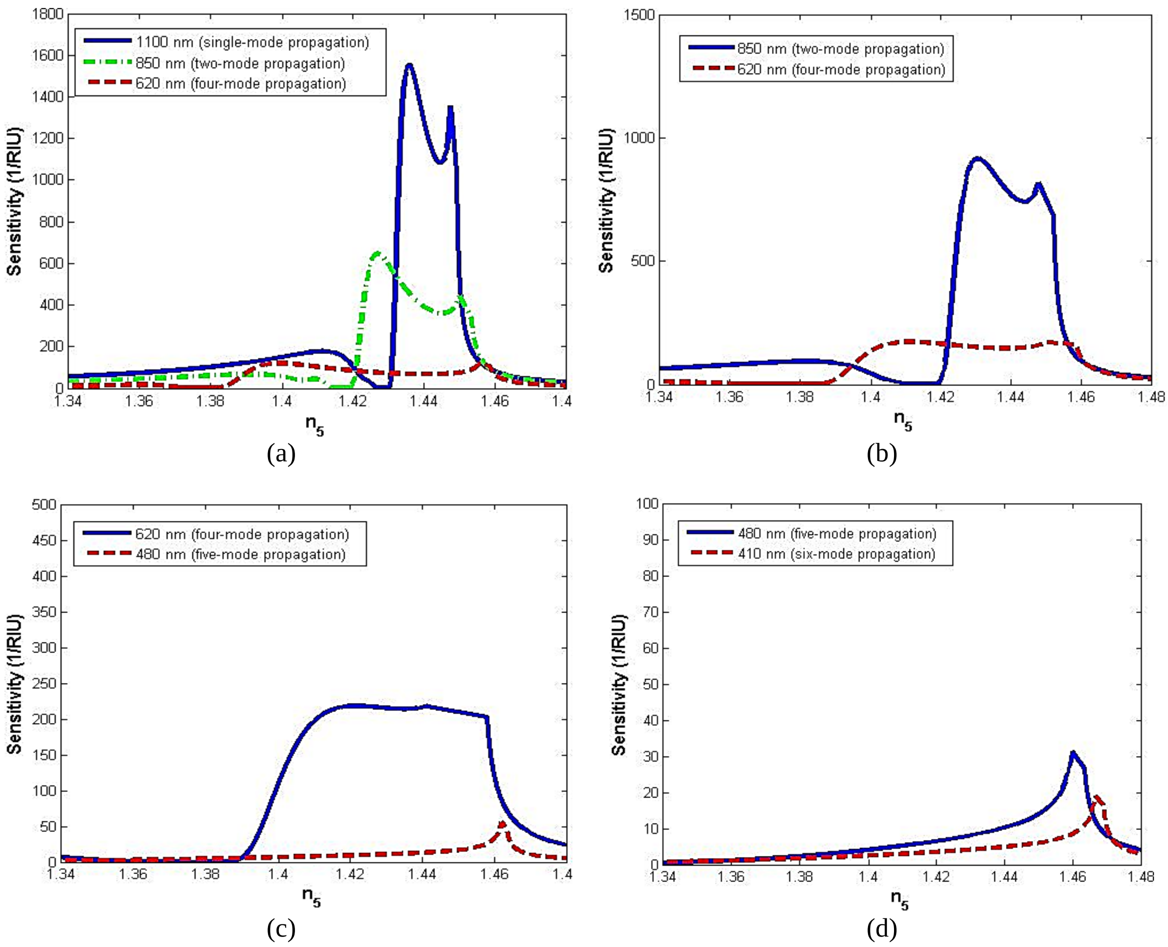

Figure 2. Performance of (a) LP_{01} (b) LP_{11} (c) LP_{21} (d) LP_{31} for different wavelengths

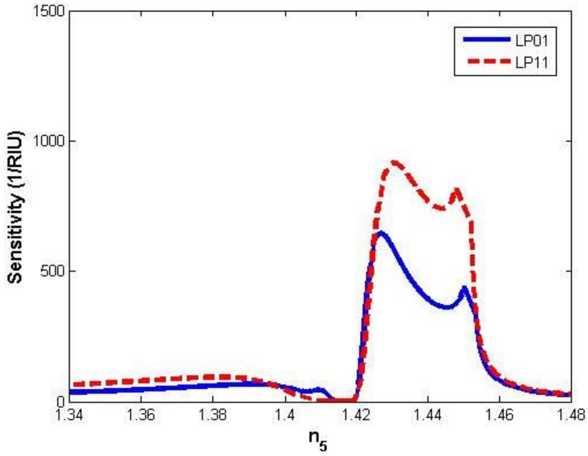

Figure 3. Performance of LP_{01} and LP_{11} in two-mode fiber operating at 850 nm

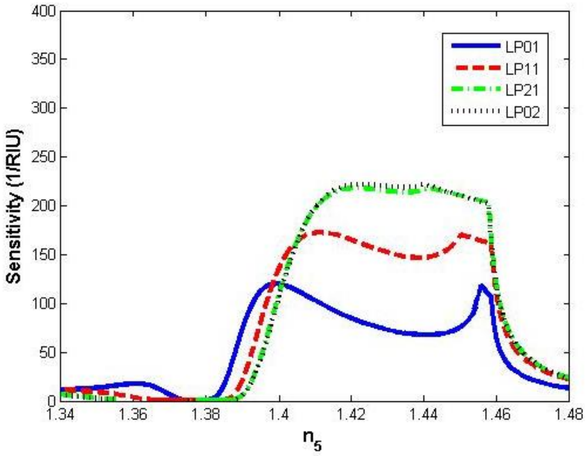

Figure 4. Performance of LP_{01}, LP_{11}, LP_{21}, and LP_{02} in four-mode fiber operating at 620 nm

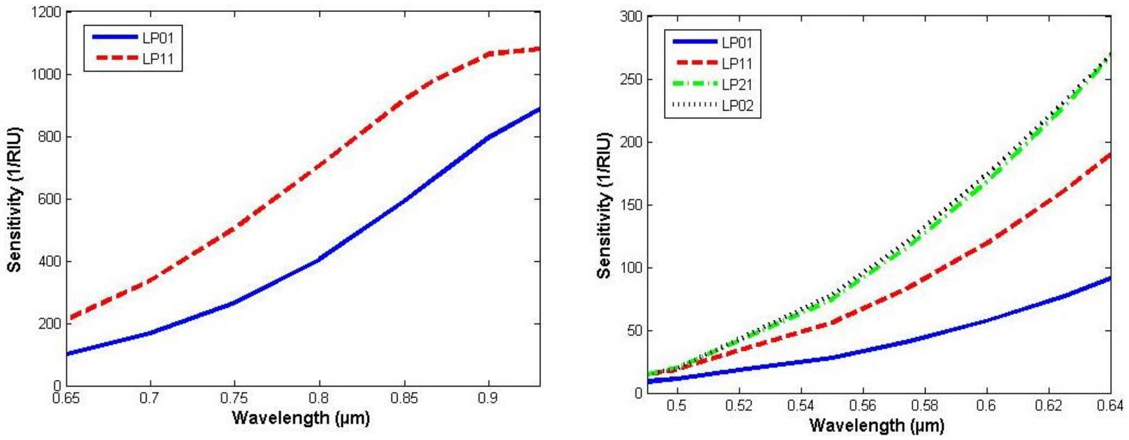

(a) (b)

Figure 5. The dependence of sensitivity on wavelength for $n_5 = 1.430$ for (a) two-mode and (b) four-mode fibers

The full width at half maximum of sensitivity (FWHM) in our case is an important parameter that indicates the range of the measured refractive index, which is desired to be as wide as possible. Although the maximum sensitivity of a particular mode decreases as the wavelength decreases, FWHM increases for that mode, which means that the range of the measured refractive index becomes wider. This is obvious from the previous figures for the modes propagated in the single-mode, two-mode, and four-mode fibers. Table 1 shows the values of maximum sensitivity, range of measured refractive index (which is taken at the half maximum of sensitivity), and FWHM for each propagating mode in single-mode, two-mode, and four-mode fibers for some selected wavelengths. For simplicity and comparison purposes, and to contribute the effect of all propagating modes, average of sensitivities maxima (sensitivity average) is determined in Table 1 for the mentioned fibers. In addition, the range of the measured refractive index and the FWHM for the mentioned fibers are determined in Table 1 according to that illustrated in Figure 6, which is related to four-mode fiber. It is noticed that the range of the measured refractive index can be determined and controlled according to the operating wavelength used. If the number of propagated modes is limited to four modes, refractive indices in subranges of 1.38 to 1.46 can be measured. A wider range can be obtained by increasing the number of propagated modes, but at the expense of sensitivity.

Tables 2 and 3 show how the previous results are affected if the core diameter is taken to be 14 and 16 μm. Comparing Tables 1 to 3, it is obvious that the sensitivity average of a fiber, that support propagation of a certain number of modes, increases as the core diameter increases. However, the range of the measured refractive index (and thus the FWHM) decreases.

Table 1. Performance parameters for single-mode, two-mode, and four-mode fibers

Fiber	Single mode	Two-mode		Four-mode			
Wavelength $[nm]$	1100	850		620			
Guided modes	LP_{01}	LP_{01}	LP_{11}	LP_{01}	LP_{11}	LP_{21}	LP_{02}
Maximum sensitivity [RIU^{-1}]	1554	645.3	915.2	120	172.6	218.2	222
Sensitivity average [RIU^{-1}]	1554	780.25		183.2			
Range of measured refractive index for each mode [RIU]	1.432 to 1.449	1.422 to 1.453	1.424 to 1.453	1.389 to 1.46	1.395 to 1.461	1.40 to 1.46	1.40 to 1.46
Range of measured refractive index for the fiber [RIU]	1.432 to 1.449	1.422 to 1.453		1.389 to 1.461			
FWHM for each mode [RIU]	0.017	0.031	0.029	0.071	0.066	0.06	0.06
FWHM for the fiber [RIU]	0.017	0.031		0.072			

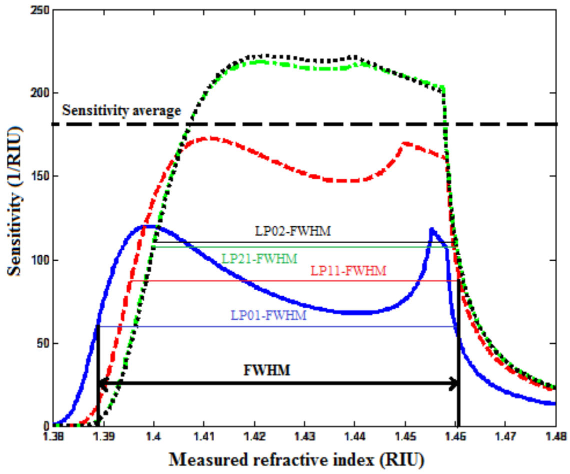

Figure 6. Determination of sensitivity average and FWHM for four-mode fiber

Choosing the core diameter depends on the range of the refractive index intended to measure. For example, according to Table 1, if the range of the refractive index intended to measure is 1.422 to 1.453 and the core diameter of the fiber is chosen to be 10 μm, then it is better to use the operating wavelength 850 nm (which supports propagation of two modes) with which a sensitivity average of 780.25 RIU^{-1} is reached (FWHM=0.031 RIU) rather than using the operating wavelength 620 nm (which supports propagation of four modes) with which a smaller sensitivity average of 183.2 RIU^{-1} is reached (FWHM=0.072 RIU). On the other hand, if the range of the refractive index intended to measure is wider, for example, 1.389 to 1.461, then it is better to operate with the 620 nm wavelength rather than the 850 nm, since the refractive indices in subranges 1.389 to 1.421 and 1.454 to 1.461 will have very small sensitivities with the 850 nm wavelength. Similarly, if the core diameter is changed, an appropriate operating wavelength can be chosen according to the refractive index range intended to measure. For example, according to Table 3, if the core diameter is chosen to be 16 μm, and the operating wavelength is chosen to be 1300 nm (to support propagation of two modes), the range of the measured refractive index will be narrower (1.434 to 1.447, FWHM=0.013 RIU), but with higher sensitivity average (1900 RIU^{-1}). The refractive indices in this range can also be measured using the 900 nm wavelength (which supports propagation of four modes), but in this case the sensitivity average will be smaller (751.68 RIU^{-1}), but on the other hand, a wider range of refractive index can be measured (1.423 to 1.452, FWHM=0.029 RIU). Thus, one of the initial steps at designing the sensor is to carefully choose the core diameter of the fiber according to the needing, where a compromise between the range of the measured refractive index and the sensitivity must be found. Figure 7 shows the sensitivity average (780.25 RIU^{-1}) and the range of the measured refractive index (1.422 to 1.453) for which the FWHM= 0.031 RIU for two-mode fiber of core diameter $d_1 = 10\,\mu m$ (at $\lambda = 850\,nm$) and how the sensitivity average increases to 1900 RIU^{-1}, while the FWHM decreases to 0.013 RIU (range: 1.434 to 1.447) when the core diameter increases to 16 μm (at $\lambda = 1300\,nm$).

The effect of changing thicknesses of residual cladding, metal layer, and graphene layer is shown in Figures 8 to 10, respectively, for the propagated modes in two-mode fiber. It can be seen in Figures 8(a) and 8(b) that changing the residual cladding thickness affects very slightly the sensitivity average and does not affect the full width at half maximum of sensitivity (FWHM), whereas changing the thickness of the metal layer affects both the average sensitivity and the FWHM as shown in Figures 9(a), 9(b) and Table 4.

Figures 10(a) and 10(b) show that the sensitivity average can be affected by changing the thickness of the graphene layer, while the FWHM remains constant.

Finally, the advantage of the technique used in this paper can be shown by comparing it with one of previous works. A refractive index SPR sensor based on photonic crystal fiber with dual coating layers is reported in [30], where a maximum sensitivity of 1739.26 RIU^{-1} is obtained (when intensity interrogation technique is used) for the measured refractive index 1.43 at the wavelength 1.58 μm. Figure 11 shows the performance of the sensor designed according to our work, where sensitivity average of 2143.5 RIU^{-1} (LP_{01} sensitivity: 1810 RIU^{-1}, LP_{11} sensitivity: 2477 RIU^{-1}) is achieved for the same measured refractive index, mentioned in the previous work, at wavelength 1.2 μm, which supports propagation of two modes (d_1,d_2,d_3,d_4, and l are taken to be 12 μm, 10 nm, 50 nm, 34 nm, and 4 mm, respectively). In addition, at the refractive index 1.431, a higher value of sensitivity average (2325 RIU^{-1}) is reached. The sensitivity average, the range of the measured refractive index and the FWHM for this sensor at the wavelength 1.2 μm are determined in Table 5. Moreover, the proposed sensor is suitable for refractive index measuring in the range 1.402-1.448 (in the case of two mode propagation) comparing to the range 1.40 to 1.44 of the mentioned previous work. Figure 12 shows the average sensitivities for the measured refractive index ranges at certain wavelengths that support propagation of two modes in the fiber.

Table 2. Performance parameters for core diameter $d_1 = 14\ \mu m$

Fiber	Single mode	Two-mode		Four-mode			
Wavelength $[nm]$	1500	1000		750			
Guided modes	LP_{01}	LP_{01}	LP_{11}	LP_{01}	LP_{11}	LP_{21}	LP_{02}
Maximum sensitivity [RIU^{-1}]	2690	838.1	1156	282.5	381.9	474.8	495.4
Sensitivity average [RIU^{-1}]	2690	997.05		408.65			
Range of measured refractive index for each mode [RIU]	1.435 to 1.444	1.429 to 1.44	1.429 to 1.45	1.411 to 1.427	1.413 to 1.455	1.414 to 1.455	1.415 to 1.455
Range of measured refractive index for the fiber [RIU]	1.435 to 1.444	1.429-1.45		1.411-1.455			
FWHM for each mode [RIU]	0.009	0.011	0.021	0.016	0.042	0.041	0.04
FWHM for the fiber [RIU]	0.009	0.021		0.044			

Table 3. Performance parameters for core diameter $d_1 = 16\ \mu m$

Fiber	Single mode	Two-mode		Four-mode			
Wavelength $[nm]$	1800	1300		900			
Guided modes	LP_{01}	LP_{01}	LP_{11}	LP_{01}	LP_{11}	LP_{21}	LP_{02}
Maximum sensitivity [RIU^{-1}]	3773	1603	2197	529.4	707.3	869.7	900.3
Sensitivity average [RIU^{-1}]	3773	1900		751.68			
Range of measured refractive index for each mode [RIU]	1.434 to 1.441	1.434 to 1.447	1.434 to 1.446	1.423 to 1.434	1.424 to 1.452	1.425 to 1.452	1.425 to 1.452
Range of measured refractive index for the fiber [RIU]	1.434 to 1.441	1.434 to 1.447		1.423 to 1.452			
FWHM for each mode [RIU]	0.007	0.013	0.012	0.011	0.028	0.027	0.027
FWHM for the fiber [RIU]	0.007	0.013		0.029			

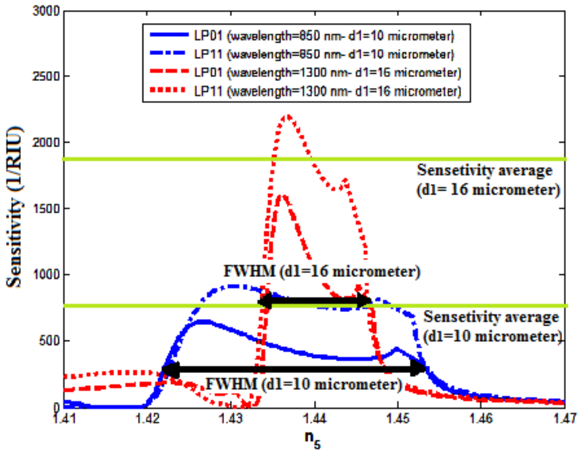

Figure 7. Modes performance in two-mode fiber of core diameter $d_1 = 10\ \mu m$ (at $\lambda = 850\ nm$) and core diameter $d_1 = 16\ \mu m$ (at $\lambda = 1300\ nm$)

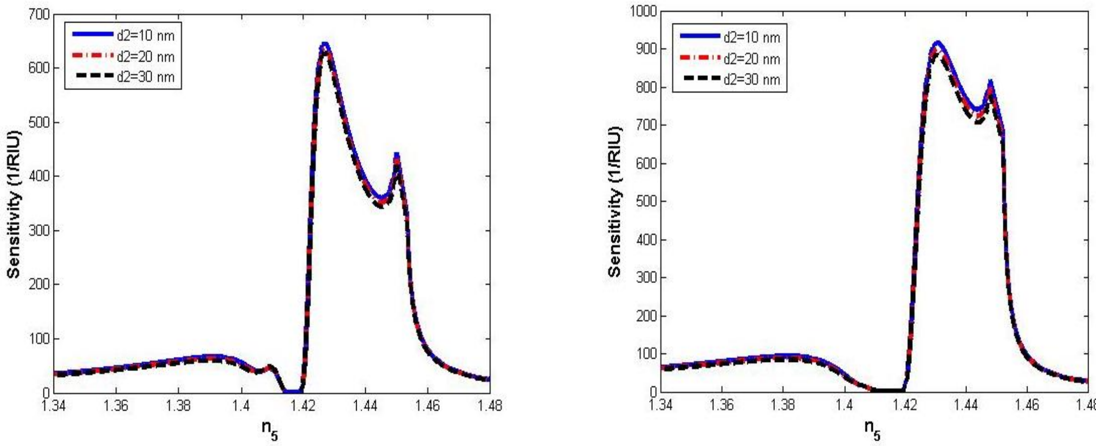

(a) (b)

Figure 8. Effect of different thicknesses of residual cladding on the performance of (a) LP_{01} and (b) LP_{11} modes in two-mode fiber ($\lambda = 850\ nm$, $d_1 = 10\ \mu m$)

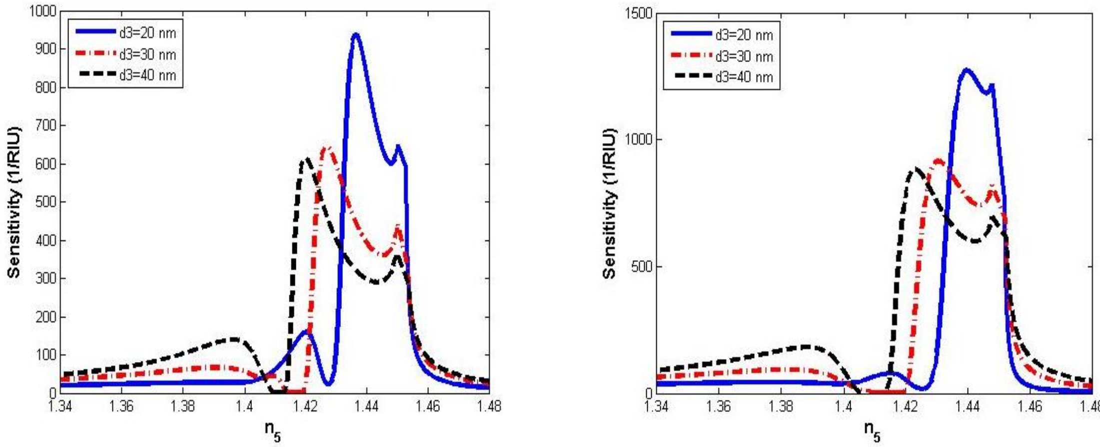

(a) (b)

Figure 9. Effect of different thicknesses of metal layer on the performance of (a) LP_{01} and (b) LP_{11} modes in two-mode fiber ($\lambda = 850\ nm$, $d_1 = 10\ \mu m$)

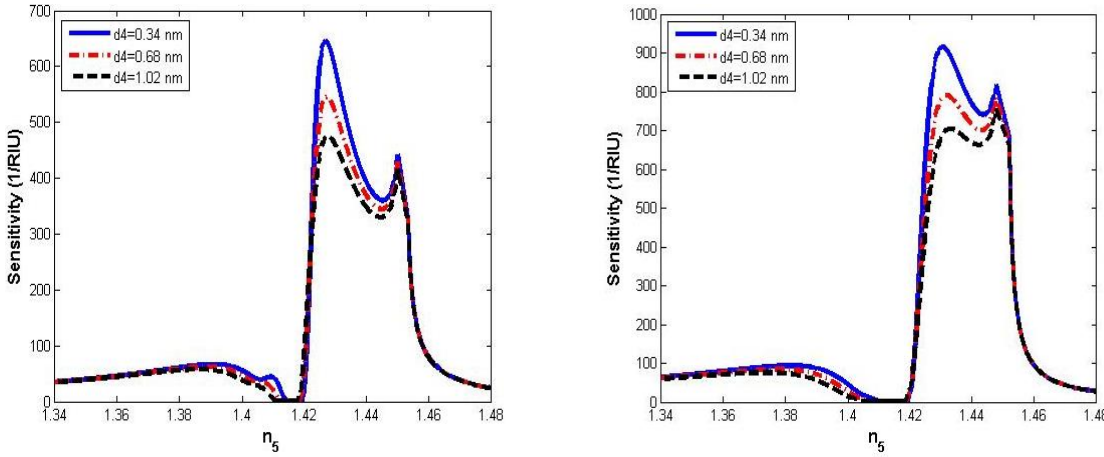

(a) (b)

Figure 10. Effect of different thicknesses of graphene layer on the performance of (a) LP_{01} and (b) LP_{11} modes in two-mode fiber ($\lambda = 850\ nm$,$d_1 = 10\ \mu m$)

Table 4. Effect of changing metal layer thickness on the two-mode fiber performance

Metal thickness [nm]	Sensitivity average [RIU^{-1}]	Range of measured refractive index [RIU]	FWHM [RIU]
20	1105	1.432 to 1.453	0.021
30	780.25	1.422 to 1.453	0.031
40	747.95	1.416 to 1.453	0.037

Table 5. Performance parameters of the two-mode fiber sensor ($\lambda = 1.2\ \mu m$, $d_1 = 12\ \mu m$)

Wavelength [nm]	1200	
Guided modes	LP_{01}	LP_{11}
Maximum sensitivity [RIU^{-1}]	1967	2683
Sensitivity average [RIU^{-1}]	2325	
Range of measured refractive index for each mode [RIU]	1.429 to 1.438	1.429 to 1.447
Range of measured refractive index for the fiber [RIU]	1.429 to 1.447	
FWHM for each mode [RIU]	0.009	0.018
FWHM for the fiber [RIU]	0.018	

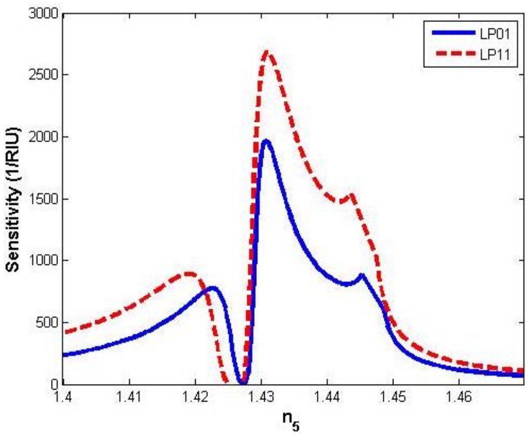

Figure 11. Performance of LP_{01} and LP_{11} in two-mode fiber ($\lambda = 1.2\ \mu m$, $d_1 = 12\ \mu m$)

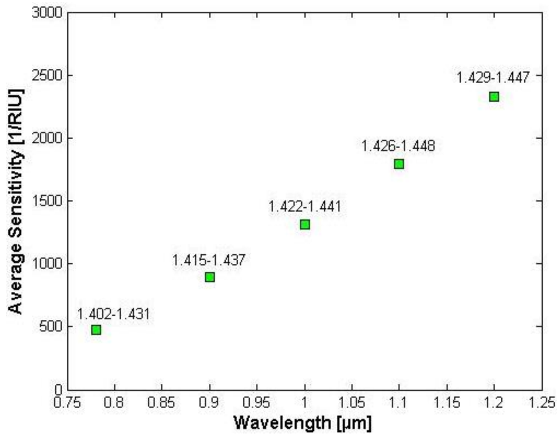

Figure 12. Average sensitivities for measured refractive index ranges at certain wavelengths

4. CONCLUSION

The performance of D-shaped SPR sensor with graphene layer has been investigated when the optical fiber supports propagation of only few modes. Sellmeier equation has been used to determine the core and cladding refractive indices, whereas the Lorentz-Drude model with two additional Lorentzian terms has been used to determine the metal refractive index. The obtained results clearly show that as the wavelength decreases, the maximum sensitivity of a particular mode decreases while the FWHM increases. Also, at certain wavelengths, comparison of sensitivities for different propagating modes has been made. It is shown that as the order of the mode increases at a certain wavelength, the value of the maximum sensitivity increases. The obtained results also show how the range of the measured refractive index can be determined and controlled according to the used operating wavelength. Refractive indices in subranges of 1.38 to 1.46 can be measured if the number of propagated modes is limited to four modes. A wider range can be obtained by increasing the number of propagated modes, but at the expense of sensitivity. Finally, it is shown that metal layer thickness has greater effect on the sensor sensitivity and FWHM than thicknesses of residual cladding and graphene layer.

REFERENCES

[1] I. Ashry *et al.*, "A review of using few-mode fibers for optical sensing," *IEEE Access*, vol. 8, pp. 179592–179605, 2020, doi: 10.1109/ACCESS.2020.3027965.
[2] M. M. A. Eid, "Optical fiber sensors: review of technology and applications," *Indonesian Journal of Electrical Engineering and Computer Science*, vol. 25, no. 2, pp. 1038–1046, Feb. 2022, doi: 10.11591/ijeecs.v25.i2.pp1038-1046.
[3] H. Hu *et al.*, "High sensitivity fiber optic SPR refractive index sensor based on multimode-no-core-multimode structure," *IEEE Sensors Journal*, vol. 20, no. 6, pp. 2967–2975, Mar. 2020, doi: 10.1109/JSEN.2019.2956559.
[4] N. Mohd Razali, P. N. S. Said Ja'afar, and S. Ambran, "Performance evaluation of a single mode optical fiber tip sensor for glucose detection," *Indonesian Journal of Electrical Engineering and Computer Science*, vol. 19, no. 3, pp. 1407–1414, Sep. 2020, doi: 10.11591/ijeecs.v19.i3.pp1407-1414.

[5] R. A. Kadhim, A.-H. Nawar, A. K. K. Abdul, L. Yuan, and J. Wu, "Optical fiber refractive index sensor based on the SPR using a multiple D-shaped Ag nanowire," in *2020 IEEE SENSORS*, Oct. 2020, pp. 1–4, doi: 10.1109/SENSORS47125.2020.9278803.

[6] N. M. Razali, A. N. Mazlan, M. F. Salebi, H. Mohamed, and S. Ambran, "Optical fiber tip sensor for glucose-adulterated honey detection," *TELKOMNIKA (Telecommunication Computing Electronics and Control)*, vol. 17, no. 5, pp. 2445–2450, Oct. 2019, doi: 10.12928/telkomnika.v17i5.12813.

[7] L. Zeni *et al.*, "A portable optical-fibre-based surface plasmon resonance biosensor for the detection of therapeutic antibodies in human serum," *Scientific Reports*, vol. 10, no. 1, Dec. 2020, doi: 10.1038/s41598-020-68050-x.

[8] R. Kant and B. D. Gupta, "Fiber-optic SPR based acetylcholine biosensor using enzyme functionalized Ta 2 O 5 nanoflakes for alzheimer's disease diagnosis," *Journal of Lightwave Technology*, vol. 36, no. 18, pp. 4018–4024, Sep. 2018, doi: 10.1109/JLT.2018.2856924.

[9] V. M. da Silva Júnior, J. F. Nascimento, and J. F. Martins Filho, "Analysis of D-shaped optical fiber based corrosion sensor using LMR and SPR effects," *Journal of Microwaves, Optoelectronics and Electromagnetic Applications*, vol. 20, no. 3, pp. 585–599, Sep. 2021, doi: 10.1590/2179-10742021v20i3254063.

[10] Pesavento, Profumo, Merli, Cucca, Zeni, and Cennamo, "An optical fiber chemical sensor for the detection of copper(II) in drinking water," *Sensors*, vol. 19, no. 23, Nov. 2019, doi: 10.3390/s19235246.

[11] V. Kapoor, N. K. Sharma, S. Gupta, and P. Kumar, "Fiber optic SPR sensing of liquids using copper and zinc oxide," *Optik*, vol. 238, Jul. 2021, doi: 10.1016/j.ijleo.2021.166727.

[12] X. Zhou, X. Li, T. Cheng, S. Li, and G. An, "Graphene enhanced optical fiber SPR sensor for liquid concentration measurement," *Optical Fiber Technology*, vol. 43, pp. 62–66, Jul. 2018, doi: 10.1016/j.yofte.2018.04.007.

[13] Z. Liu *et al.*, "SPR sensor based on bessel-like beam," *Optics Express*, vol. 29, no. 12, Jun. 2021, doi: 10.1364/OE.423760.

[14] G. Melwin and K. Senthilnathan, "High sensitive D-shaped photonic crystal fiber sensor with V-groove analyte channel," *Optik*, vol. 213, Jul. 2020, doi: 10.1016/j.ijleo.2020.164779.

[15] Y. Wei *et al.*, "Optical fiber cladding SPR sensor based on core-shift welding technology," *Sensors*, vol. 19, no. 5, Mar. 2019, doi: 10.3390/s19051202.

[16] W. Udos *et al.*, "Label-free surface-plasmon resonance fiber grating biosensor for hand-foot-mouth disease (EV-A71) detection," *Optik*, vol. 228, Feb. 2021, doi: 10.1016/j.ijleo.2020.166221.

[17] M. Lobry *et al.*, "Multimodal plasmonic optical fiber grating aptasensor," *Optics Express*, vol. 28, no. 5, Mar. 2020, doi: 10.1364/OE.385747.

[18] A. Bekmurzayeva *et al.*, "Etched fiber Bragg grating biosensor functionalized with aptamers for detection of thrombin," *Sensors*, vol. 18, no. 12, Dec. 2018, doi: 10.3390/s18124298.

[19] D. T. Nurrohman and N.-F. Chiu, "A review of graphene-based surface plasmon resonance and surface-enhanced Raman scattering biosensors: Current status and future prospects," *Nanomaterials*, vol. 11, no. 1, Jan. 2021, doi: 10.3390/nano11010216.

[20] A. K. Paul, M. A. Mollah, M. Z. Hassan, N. Gomez-Cardona, and E. Reyes-Vera, "Graphene-coated highly sensitive photonic crystal fiber surface plasmon resonance sensor for aqueous solution: design and numerical analysis," *Photonics*, vol. 8, no. 5, May 2021, doi: 10.3390/photonics8050155.

[21] W. Gong *et al.*, "Experimental and theoretical investigation for surface plasmon resonance biosensor based on graphene/Au film/D-POF," *Optics Express*, vol. 27, no. 3, Feb. 2019, doi: 10.1364/OE.27.003483.

[22] H. Yu, Y. Chong, P. Zhang, J. Ma, and D. Li, "A D-shaped fiber SPR sensor with a composite nanostructure of MoS2-graphene for glucose detection," *Talanta*, vol. 219, Nov. 2020, doi: 10.1016/j.talanta.2020.121324.

[23] W. F. Abu Shehab, "Performance analysis of optical fiber surface plasmon resonance sensor in single-mode operation region," *Journal of Electrical Engineering*, vol. 71, no. 5, pp. 340–346, Sep. 2020, doi: 10.2478/jee-2020-0046.

[24] L. Kong, J. Lv, Q. Gu, Y. Ying, X. Jiang, and G. Si, "Sensitivity-Enhanced SPR Sensor Based on Graphene and Subwavelength Silver Gratings," *Nanomaterials*, vol. 10, no. 11, Oct. 2020, doi: 10.3390/nano10112125.

[25] A. Mendez and T. F. Morse, *Light-guiding fundamentals and fiber design*. California, USA: Academic Press, 2007.

[26] D. Bayuwati and T. B. Waluyo, "Macro-bending loss of single-mode fiber beyond its operating wavelength," *TELKOMNIKA (Telecommunication Computing Electronics and Control)*, vol. 16, no. 1, pp. 142–150, Feb. 2018, doi: 10.12928/telkomnika.v16i1.6666.

[27] R. Chlebus, J. Chylek, D. Ciprian, and P. Hlubina, "Surface plasmon resonance based measurement of the dielectric function of a thin metal film," *Sensors*, vol. 18, no. 11, Oct. 2018, doi: 10.3390/s18113693.

[28] B. E. A. Saleh and M. C. Teich, *Fiber optic*. NJ, USA: John Wiley & Sons, 2019.

[29] M. F. Ubeid and M. M. Shabat, "Numerical investigation of a D-shape optical fiber sensor containing graphene," *Applied Physics A*, vol. 118, no. 3, pp. 1113–1118, Mar. 2015, doi: 10.1007/s00339-014-8925-y.

[30] D. Li, W. Zhang, H. Liu, J. Hu, and G. Zhou, "High sensitivity refractive index sensor based on multicoating photonic crystal fiber with surface plasmon resonance at near-infrared wavelength," *IEEE Photonics Journal*, vol. 9, no. 2, pp. 1–8, Apr. 2017, doi: 10.1109/JPHOT.2017.2687121.

BIOGRAPHIES OF AUTHORS

Wael Abu Shehab received the M.Sc. and Ph.D. degrees in Electronics and Telecommunication Technique from VSB-Technical University of Ostrava, Czech Republic, in 1997 and 2001, respectively. From 2001 to 2009, he was a lecturer and the head of the Department of Industrial Electronics and Control at Jazan College of Technology, Saudi Arabia. Since 2010, he has been with Al-Hussein Bin Talal University at Ma'an, Jordan, where he is currently an Associate Professor at the Department of Electrical Engineering. His research interest spans a wide range of topics including optical fiber sensors, wireless communications, and electrical networks. He can be contacted at waelabushehab@ahu.edu.jo.

Ahmad Salah received the B.Eng. degree in Electrical Engineering from the Yarmouk University, Irbid, Jordan, in 2008, the M.Sc. degree in Electrical and Computer Engineering from the New York Institute of Technology, Amman, Jordan, in 2012, and the Ph.D. degree from the University of Technology Sydney, Ultimo, NSW, Australia, in 2018. From 2018 to 2022, he held several academic positions in both Australian and Jordan universities. Since 2019, he has been an Assistant Professor of Electrical Engineering with Al-Hussein Bin Talal University, Maan, Jordan and the Chair of the Electrical Engineering Department. His research interests include condition monitoring and fault detection in induction machines and renewable energy control systems. He can be contacted at ahmad.salah@ahu.edu.jo.

Wael Al-Sawalmeh received the M.Sc. degree in Electrical and Communication Engineering from Leningrad, Electro Technical Institute of Communications named after Bonch-Bruyevitch, Russia, in 1993. He Received the Ph.D. degree in Electrical and Communication Engineering from University of Telecommunication at Saint-Petersburg, Russia, in 1998. Since Aug. 1999, he served in many universities at Libya, and from 2011 until present, he worked as a full-time lecturer in Al- Hussein Bin Talal University at Ma'an, Jordan, where he is currently an Associate Professor. His research spans a wide range of topics including signal and image processing and information theory. He can be contacted at walsawalmeh@ahu.edu.jo.

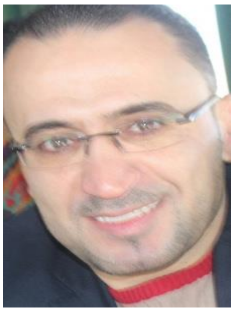

Haitham Alashaary received the B.S. degree in Electronics Engineering from the Yarmouk University, Irbid, Jordan, in 2000, the M.Sc. degree in Biomedical Engineering from the University of New South Wales, Australia, in 2003, and the Ph.D. degree in Electrical and Computer Engineering from the University of Newcastle, Australia in 2010. He is currently an Associate Professor and the Head of Computer Engineering Department at Al-Hussein Bin Talal University, Jordan. His research interests include, but not limited to, neural networks; fuzzy logic; neuro-fuzzy techniques; signal and image processing; automatic control; parallel computing; electronics. He can be contacted at haitham.alashaary@ahu.edu.jo.